

## AN IMPULSE RESPONSE TECHNIQUE TO IMPROVE THE EFFECTIVE FREQUENCY RESPONSE OF PRESSURE PROBES

D. Burdett, R. Lubbock, T. Povey

Osney Thermofluids Laboratory, University of Oxford  
 OXFORD, OX2 0ES, UK

**Keywords:** frequency response, pressure probes, impulse response technique

### ABSTRACT

Probes used for aerodynamic surveying (e.g. pneumatic pressure probes) have frequency response characteristics that generally limit either the temporal scale that can be resolved (for example, for a fixed probe flow unsteadiness cannot be resolved beyond a certain frequency limit) or the physical scale that can be resolved (for example, a traversing probe moving at a fixed speed through a spatially varying field). In this paper, impulse response deconvolution techniques—familiar to the heat transfer research community—are used to improve the effective frequency response characteristics of both pressure and temperature probes. This technique allows a probe to resolve flow unsteadiness to frequencies or wavenumbers higher than the ‘natural’ limit of the probe, expanding the frequency and wavenumber ranges over which probes can be used. The technique has wide application in aerodynamic surveying applications where spatial or temporal resolution is limited by probe frequency response.

The technique is demonstrated using experimental data from a high-speed turbine experiment. Aerodynamic survey data were collected in a series of experiments with traverse speeds both above and below the effective wavenumber limit of the probe. The technique has been demonstrated using pneumatic pressure probes, but in principle could be applied to any probe for which the impulse response can be characterised by analytical, numerical or experimental means. Impulse response deconvolution techniques are used to reconstruct data beyond the natural frequency limit, demonstrating the method and establishing practical limits on the accuracy that can be achieved when applying the method in realistic experimental environments.

### NOMENCLATURE

#### Romans

$A = \pi d^2/4$	Cross-sectional area of connecting tube
$\bar{a}$	Mean speed of sound
$b$	Variable defined in [14, 17]
$D_n$	Dissipation number
$d$	(Inner) diameter of connecting tube

$f_0$	Natural frequency
$f_s$	Sample frequency
$h$	Impulse response function
$i$	Summation variable
$l$	Length of connecting tube
$N$	Number of points in sampled signal
$n$	Sample number
$n_T$	Polytropic exponent in transducer cavity
$p$	Input pressure signal
$p'$	Output pressure signal
$\bar{p}$	Mean pressure
$p_1$	Pressure signal measured at speed $v_1$
$p_2$	Pressure signal measured at speed $v_2$
$Q$	Volume flow rate
$r$	Step response function
$s$	Laplace frequency variable
$t$	Time
$u$	Unit step function
$v$	Velocity
$x$	Space variable
$y$	Variable defined in [14, 17]
$Z_0$	Impedance constant
$Z_c$	Characteristic impedance
$Z$	Variable defined in [14, 17]

#### Greeks

$\alpha$	Variable defined in [14, 17]
$\beta$	Variable defined in [14, 17]
$\Gamma$	Propagation constant
$\gamma$	Ratio of specific heats
$\delta$	Unit impulse function
$\lambda_{ci}$	Root index
$\mu$	Mean dynamic viscosity
$\nu$	Mean kinematic viscosity
$\xi$	Damping ratio
$\rho$	Mean mass density
$\tau$	Time constant
$\varphi$	Dummy variable in convolution integrals

### INTRODUCTION

The frequency response of probe systems places a limit on the spatial or temporal resolution of data that can be obtained in aero-thermal surveying applications.

For pneumatic pressure probes used for aerodynamic measurement, the natural frequency limit is a function of probe design, the connecting tubing geometry, and the transducer internal

volume. For thermocouple probes, the natural frequency limit is a function of the flow speed around the thermocouple bead (sometimes artificially reduced for structural reasons, as in the case of aspirated probes), the thermal mass of the bead, and the geometry with respect to the flow. Corrections may also be necessary for the thermal conductivity of the wire support and for surrounding radiation.

For the case of traverse measurements through a spatially and temporally steady pressure field, the temporal pressure signals recorded by the probe, or *observed signal*,  $p'(t)$ , can be thought of as being convolved (or filtered) with the probe system impulse response filter. The *underlying signal*,  $p(t)$ , is recovered by deconvolving  $p'(t)$  and the probe impulse response.

The practical effect of the finite probe system response time on the observed signal with increasing probe traverse speed is twofold: to impose increasing spatial shifts in the data in the direction of probe travel; and to lower the peak height when the probe passes through a spatial excursion in pressure (e.g. in turbomachinery applications, a vane wake). This effect is illustrated in Figure 1. For an identical underlying signal measured at four different traverse speeds (a nominal speed  $v$  and higher speeds,  $5v$ ,  $10v$  and  $20v$ ) the disagreement between observed signals from traverses in opposite directions increases with traverse speed.

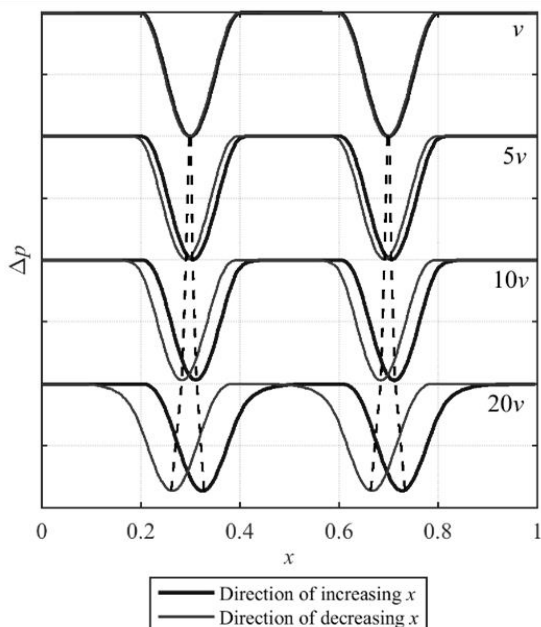


Figure 1: Example pressure traverse signals traversed at four different speeds and in two directions

Two-dimensional traverse maps and area contour plots are typically built up from alternating traverses in different directions. For relatively high traverse speeds (e.g. the  $20v$  traverse speed) this results in non-physical alternating shifts in wake

position as illustrated in Figure 2. Reducing the traverse speed until this effect becomes negligible is often undesirable, particularly in short duration test facilities where run time is limited, or where the cost of an individual test is significant.

For pressure measurement probes, the length of connecting tubing between the probe tip and the transducer could also be reduced, but this is often limited by practical constraints in locating the transducers in the experimental facility. In general, it is advantageous to be able to recover the underlying signal with as high a frequency response as possible, thus extending the effective bandwidth for fixed probes, and the effective spatial resolution for moving probes.

Holmes and Lewis [1] improved the frequency response of pressure probe systems by inserting small diameter restrictions into the connecting tubing. Van Ommen et al [2] considered the dy response of a pressure probe-transducer system in the frequency domain and used this to optimise probe design for a specific application. Hooper and Musgrove [3] and Paniagua and Dénos [4] used an inverse transfer function method to compensate the frequency response of pressure probe systems. In the latter case the impulse response function was determined by fitting a linear system to an experimentally determined time-response.

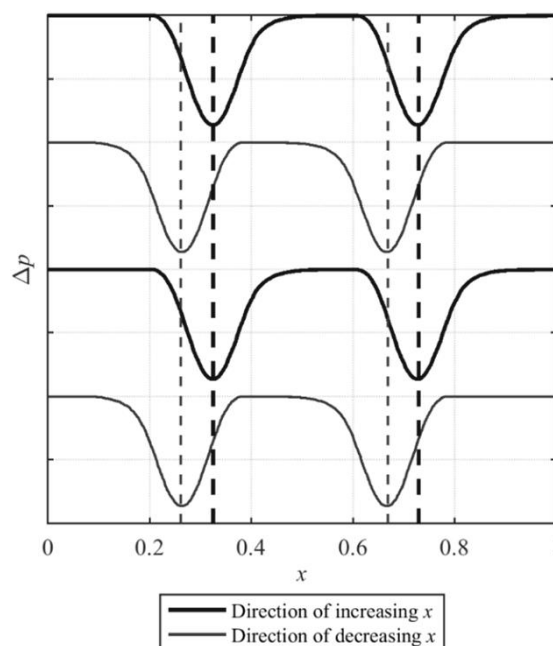


Figure 2: Example of the spatial shifting of data in a 2D traverse plane due to frequency response limitations

A number of previous studies [5, 6, 7] have attempted to improve the frequency response of temperature probes by using two thermocouple junctions of differing diameters on a single probe. Braun et al [7] use this method to predict the response of a virtual third junction of smaller

diameter, and obtain a 14-fold increase in bandwidth limit.

A processing technique familiar to the heat transfer community is Oldfield's impulse response deconvolution method [8], which can be used to establish the unsteady heat flux to a substrate surface from the substrate surface transient temperature history. The substrate surface temperature history characteristically has limited bandwidth (damped by the thermal inertia of the substrate) in comparison to the underlying incident heat flux signal, which is unfiltered and therefore includes the full spectrum of frequencies up to the Nyquist limit. The underlying heat flux signal can be *recovered* by deconvolution of the temperature signal and the substrate surface temperature impulse response. The impulse response is derived by deconvolving a pair of substrate basis functions, such as the temperature response to a unit step in heat flux. These basis functions may be derived analytically, numerically or experimentally, although the former is the most straightforward if a suitable mathematical model exists. In this manner, a relatively high frequency temporal heat flux signal is recovered from the relatively low frequency substrate surface temperature signal.

To calculate the substrate surface *impulse response*, a pair of corresponding input-output transients for the system are required, for example, the transient response of the substrate surface,  $T(t)$ , when subject to a unit step change (in time) in heat flux. For a given system, the input-output pair could be analytically derived, determined experimentally (e.g. a step change in heat load is applied, for example by a laser or suitable transient convection facility [9]), or derived numerically using an appropriate numerical model [10]. Once the particular impulse response for the system is known, a digital filter can be created to deconvolve the filtered output signal to recover the higher frequency input signal. A similar method was used by Stepanishen and Fisher [11] for processing experimental measurements of the acoustic field of pulsed ultrasonic radiators.

This paper is concerned with the practical application of the impulse response method to pressure measurements typical for aerodynamic traversing probes. Three different methods for generating the required impulse response filter are compared for the cases of a multi-hole pneumatic pressure probe and a thermocouple probe. The methods are:

1) *Theoretical system models*. Analytical models which use as inputs the physical geometry and fluid properties of the system. We compare several models and comment on the results.

2) *Experimental step-response characterisation*. The response of the system to a step change in

pressure is measured directly (e.g. using the *balloon method*, described later).

3) *Multi-experiment in-situ characterisation*. A number of experiments are conducted in which data is acquired at different traverse speeds and the impulse response of the system is determined as the function which best reduces the data to a common input signal.

In each case the application of the technique to traverse data taken in a high speed experimental facility downstream of an annular cascade of high pressure nozzle guide vanes is demonstrated.

## IMPULSE RESPONSE TECHNIQUE

The impulse response processing technique [8, 12] requires a discrete transfer function—sampled at the same rate as the data to be processed—which describes the transformation required to recover an input signal from a known output. The transfer function is applied to the data in the form of a digital filter. The technique can be used for any linear time-invariant (LTI) system.

Consider the pressure measurement system comprising probe, connecting tubing and transducer cavity shown in Figure 3. The system has an underlying signal (true input pressure signal at the intended measurement location),  $p(t)$ , and an observed signal (the output, measured at the transducer sensing element),  $p'(t)$ .

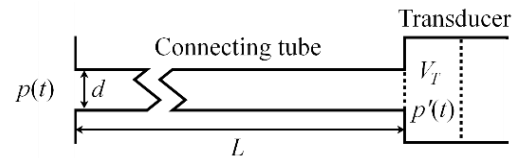


Figure 3: A typical pressure measurement system

The system transfer function is given by the convolution integral

$$p'(t) = h(t) * p(t) = \int_{-\infty}^{\infty} h(\varphi) p(t - \varphi) d\varphi \quad (1)$$

where  $h(t)$  is the response of the system to a unit impulse at time  $t = 0$ . This is equally valid using any independent axis variable—as will be shown in later sections the method can be applied either on a temporal basis or on a spatial basis. For example

$$p'(x) = h(x) * p(x) = \int_{-\infty}^{\infty} h(\varphi) p(x - \varphi) d\varphi \quad (2)$$

where  $h(x)$  is the response of the system to a unit impulse at position  $x = 0$ . The continuous time signals are sampled at discrete time intervals with frequency  $f_s$

$$p[n] = p\left(t = \frac{n}{f_s}\right) \quad \forall n \in \mathbb{Z} \quad (3)$$

The convolution integral describing the system transformation thus becomes a discrete convolution sum

$$p[n] = h[n] * p'[n] = \sum_{i=1}^N h[i] p'[n-i] \#(4)$$

The input signal can be recovered from the recorded output signal by inverting the convolution sum

$$p[n] = (h[n])^{-1} * p'[n] = \sum_{i=1}^N (h[i])^{-1} p'[n-i] \#(5)$$

These two operations are depicted in Figure 4. The discrete convolution of equation 5 can be performed using the MATLAB function *fftfilt*, digitally filtering the system output signal,  $p_o[n]$ , using the inverse impulse response function as the filter window function.

Correcting for the response of a specific system therefore requires that an appropriate sampled *inverse* impulse response function,  $(h[n])^{-1}$ , is determined. This is achieved by starting from a known pair of input-output functions and applying the above method in reverse. The most straightforward—but not the only applicable—pair is a unit step function,  $u[n]$ , and unit step response function,  $r[n]$ . By definition

$$r[n] = h[n] * u[n] \Rightarrow h[n] = r[n] /* u[n] \#(6)$$

where  $/*$  denotes a deconvolution operation. Inverting equation 6 to obtain the inverse response function

$$(h[n])^{-1} = u[n] /* r[n] \#(7)$$

Both sides of equation 7 can be convolved with a unit impulse function without affecting the result

$$(h[n])^{-1} * \delta[n] = (u[n] /* r[n]) * \delta[n] \#(8)$$

Finally, reformulating equation 8 as a discrete convolution sum

$$(h[n])^{-1} = \sum_{i=1}^N \frac{u[i]}{r[i]} \delta[n-i] \#(9)$$

Hence the inverse impulse response function is determined by digitally filtering a unit impulse (Dirac delta) function with filter coefficients given by the ratio of the input-output transform pair of functions. The impulse response filter is specific to a given LTI system, and need only be determined once. It can then be applied to any output data from that system.

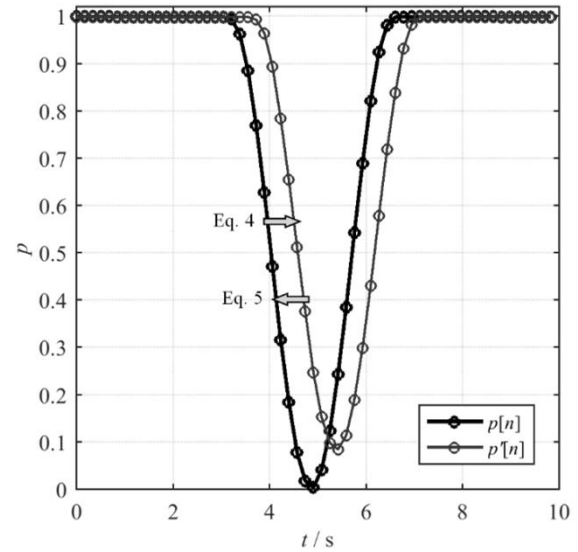


Figure 4: Idealised system input and output pressure signals, illustrating the transformations performed by Equations 4 and 5

## METHODS FOR CONSTRUCTING IMPULSE RESPONSE FILTER

To enable comparison of impulse response filter generation techniques, an example system is referenced which is typical of a pressure probe used in turbomachinery experiments. The system is defined by: 30 mm length of 0.45 mm internal diameter tube (representing the probe tip); 500 mm of 1.00 mm internal diameter tube (representing the connecting tube); 20.3 mm<sup>3</sup> dead volume (representing the transducer diaphragm cavity).

The three methods for constructing the impulse response filter are now considered in turn (Theoretical system models; Experimental characterisation of system step response (balloon test); Method 3: In-situ experimental determination of spatial impulse transformation function).

### Method 1: Theoretical system models

In many cases it is helpful to be able to construct the impulse response function of the measurement system using a purely theoretical approach. For example, for an aerodynamic probe, the inputs would be the probe-system geometry and fluid properties. Where this technique is possible, no additional experiments are required.

There are a number of theoretical models of pressure probe / transducer systems available in the literature. Three theoretical models are described here.

Bajsić et al [13] describe a simple second order model in the form of a Helmholtz resonator—effectively modelling the air in the connecting tube and transducer cavity as a mass oscillating in 1D

$$\frac{d^2 p'}{dt^2} + 4\pi\xi f_0 \frac{dp'}{dt} + 4\pi^2 f_0^2 p' = 4\pi^2 f_0^2 p \#(10)$$

The natural frequency is given by

$$f_0 = \frac{\bar{a}}{2\pi} \sqrt{\frac{A}{lV_T}} \#(11)$$

The damping ratio is estimated as

$$\xi = \frac{2\mu}{\rho A f_0} \#(12)$$

Results using these relations were compared with experimental measurements [13] for a range of tube lengths and diameters. The values of natural frequency were found to be in excellent agreement. While the trends in damping ratio with changes in both tube length and diameter were well predicted, the absolute values were significantly underestimated. A simple model of this type may require tuning to optimise its agreement with experimental data for a particular system. In particular the value of damping ratio may be better set by taking a value to match experimental data. The damping ratio is especially sensitive to small changes in the probe system geometry which may be poorly realised in such a simple model.

This model will be referred to as *Model 1*. Figure 5 shows resulting step response functions obtained by applying Model 1 to the example pressure probe system. The value of damping ratio predicted by Equation 12 was 0.761, while the value found by matching the response to experimental data was 0.725, a deviation of 4.7%. This results in a 1.1% increase in peak overshoot before the response settles to unity. The predicted value of  $\xi$  is therefore an acceptable approximation. Hall and Povey [14] note that simple models of this type tend to provide stronger agreement with experimental data in underdamped cases than in overdamped cases.

Hall and Povey [14] compare a number of existing models for pressure probe system response and detail the development of a new model designed to be both accurate and simple to implement. These models describe the probe-transducer system as a fluidic transmission line, modelling each section of tubing as a transmission line with an associated loss, and intermediate volumes as reservoirs. Considering the characteristic properties of the line to be distributed over a series of infinitesimally small repeating units yields a transfer matrix representation of the line

$$\begin{bmatrix} P \\ Q \end{bmatrix} = \begin{bmatrix} \cosh(\Gamma l) & -Z_c \sinh(\Gamma l) \\ -\left(\frac{1}{Z_c}\right) \sinh(\Gamma l) & \cosh(\Gamma l) \end{bmatrix} \begin{bmatrix} P' \\ Q' \end{bmatrix} \#(13)$$

This formulation is used in the equivalent models of Bergh and Tidjeman [15] and Richards [16] and allows much more accurate prediction of the harmonic response than simpler models. The definition of the propagation constant,  $\Gamma$ , is given in [14] and features Bessel functions, making the solution impossible to find analytically. Equation 13 can be solved numerically for a system with an arbitrary number of tube sections of different lengths and diameters, to obtain the step response function. This will be referred to as *Model 2*.

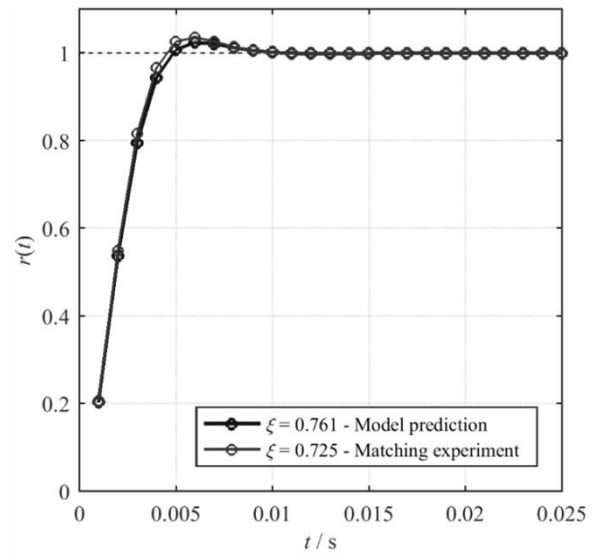


Figure 5: Step response functions from Model 1 for two different damping ratios

Alternatively, Equation 13 can be simplified using the modal approximation of Yang and Tobler [17] in the Laplace frequency domain to obtain a low (second) order transfer function describing the probe system response (Equation 14). This is far more convenient than the direct numerical solution of Equation 13. Definitions of the variables ( $b, D_n, y, z, Z_0, \alpha, \beta, \lambda_{ci}$ ) in Equation 14 can be found in [14, 17]. This will be referred to as *Model 3*. Equation 14 can be solved analytically to obtain the step response function for the example measurement system, shown in Figure 6.

$$\frac{P'(s)}{P(s)} = \frac{\frac{\pi}{4}}{\frac{\alpha^2 d^2}{16v\lambda_{ci}} \left( \frac{d^2 D_n}{32v} + \frac{yV_T Z_0}{zn_T \bar{p}} \right) s^2 + \left[ \frac{\pi\alpha\beta d^2 D_n}{16v\lambda_{ci}} + \frac{\pi V_T Z_0}{4zn_T \bar{p} \lambda_{ci}} (8\alpha\beta y + (\alpha - \gamma)b\lambda_{ci}^2) \right] s + \frac{D_n \lambda_{ci}}{2}} \#(14)$$

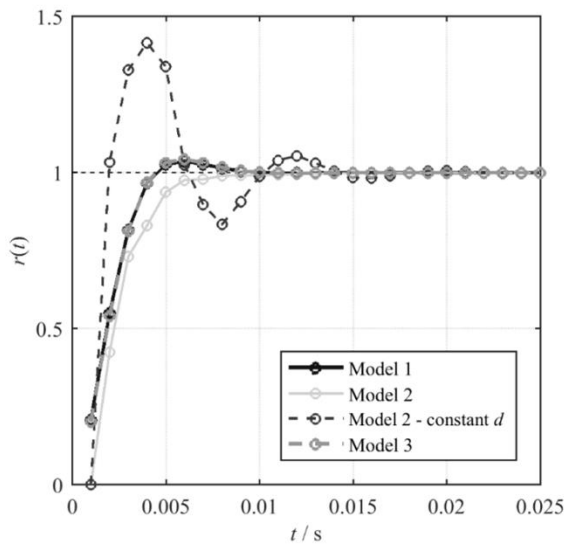


Figure 6: Step response functions from all theoretical models

Figure 6 shows step response curves for the example pressure probe system from all theoretical models. The responses from the two low order models (Models 1 and 3) collapse onto one another, showing that they give almost identical descriptions of the system. This illustrates the utility of the very simple Equations 11 and 12. The response from Model 2 has a similar settling time to the other models but has no overshoot. There are additional small-scale features due to the ability of the model to predict system harmonic frequencies.

The response curve obtained by applying Model 2 to the example pressure probe system assuming a constant tube diameter (i.e. disregarding the short probe tip) is also plotted. This is less damped than that using Model 2, rising to a peak overshoot of 41% of step height. The probe tip, being the section of minimum tube diameter, therefore sets the damping for the entire system.

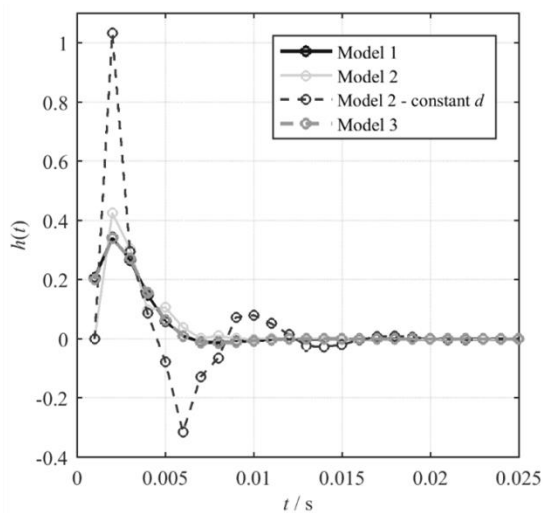


Figure 7: Impulse response functions from Models 2 and 3

Corresponding impulse response functions, calculated from Equation 9, are plotted in Figure 7. The inverses of these functions give the discrete impulse response filters which will be applied according to Equation 5.

### Method 2: Experimental characterisation of system step response (balloon test)

A pressure probe-system response characteristic can be measured directly via an experimental technique referred to as the *balloon method*.

A diagram of the test setup is shown in Figure 8. The tip of the probe-system is arranged inside a latex balloon in close proximity to a pressure transducer with flush mounted diaphragm (giving a frequency response of the order  $10^4$  Hz). The tubing connecting the probe-system to transducers should be of the same length and type as in the experimental system being characterised, or ideally the test should be performed in-situ. By inflating the balloon to failure, an almost perfect step input in pressure (approximately -0.12 bar) is achieved. The bare transducer is used to characterise the input step. The output signal from the probe-system is also measured, giving a known input-output pair of basis functions from which the system impulse response filter can be calculated. The method is simple to implement in practice, and removes uncertainties associated with simplifications in theoretical approximations.

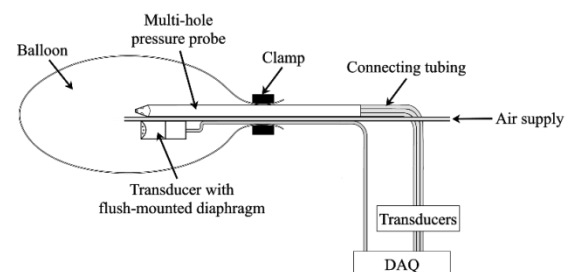


Figure 8: Diagram of the setup of the experimental balloon test

Figure 9 shows the resulting signals. The input step is covered within one sample in the bare transducer signal. Ideally the sample rate for the test should be maximised to resolve the input step as far as possible. The probe output signal is averaged over three individual measurements (shown as faint lines in Figure 9) made simultaneously using different ports on the probe tip, and has the form of a moderately overdamped system, reaching 95% of the step height after 8 ms. This compares well with the step response function derived from theoretical Model 2 in the previous section, with evidence of similar high frequency components.

The corresponding impulse response functions are plotted in Figure 10, using both the signal measured by the bare flush-mounted transducer and a perfect unit step as the reference input signal. The general shape of the functions is very similar. There is a mismatch in the first two samples due to the overshoot on the reference signal. The transfer function from the bare transducer signal has noticeably less noise once settled, as the high frequency components interfere destructively between the two signals.

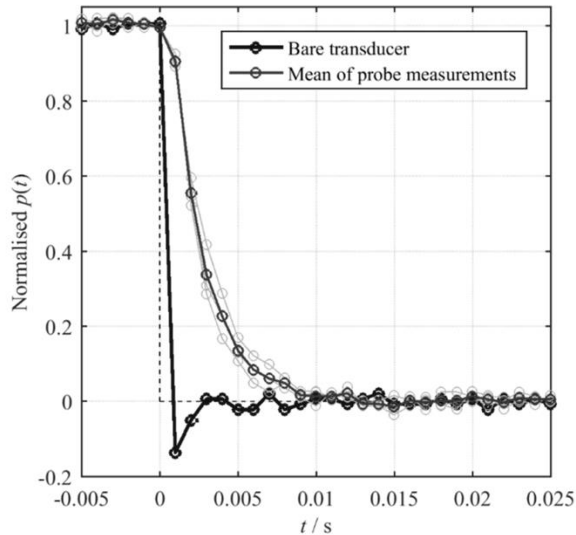


Figure 9: Step response result from Method 2

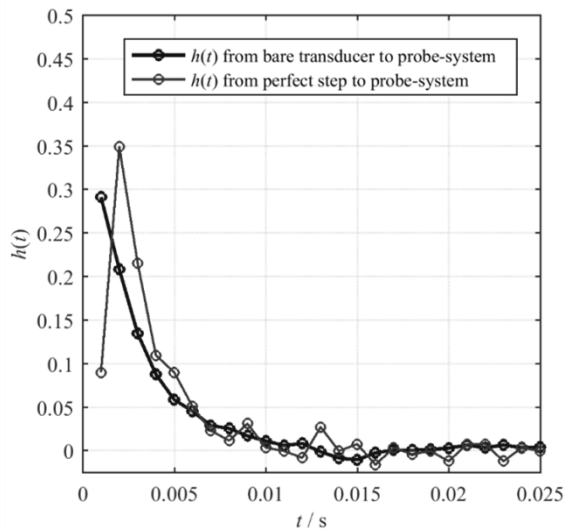


Figure 10: Impulse response functions derived from Method 2

### Method 3: In-situ experimental determination of spatial impulse transformation function

As discussed, any input-output basis function pair can be used to construct the impulse response filter. Examples for a unit-step/unit-step-response pair have been demonstrated but in principle any signal pair with an input signal including frequency

content up to the highest frequency of interest would suffice. For example, an impulse response function could be generated from corresponding input-output pairs of traverse signals generated by surveying the same steady-state flow field at a number of different traverse speeds. This approach is demonstrated in this section.

Consider two traverses of the same flow conducted at speeds  $v_1$  and  $v_2$ . For a very low speed  $v_1$ , the observed signal closely approximates the underlying signal. At a higher speed  $v_2$ , representing a desired traverse speed, the observed and underlying signals may differ. The correct system transfer function is that which corrects the observed signal at speed  $v_2$  to the observed signal at speed  $v_1$ . The effective frequency response is therefore enhanced beyond the natural limit of the probe system at speed  $v_2$ . The slower the first traverse can be made, the higher the resolution of the recovered signal that can be achieved (up to the limit of the maximum frequency in the underlying signal). This method is equally applicable to pressure, temperature, and any other variable which can be measured over a 1D traverse.

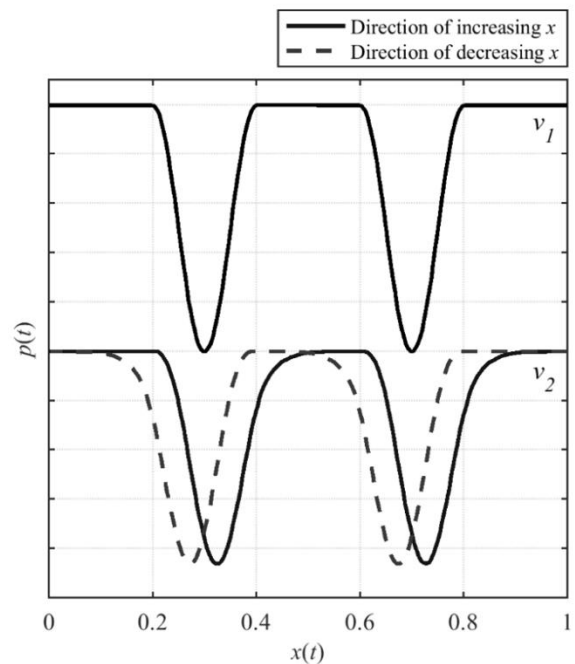


Figure 11: Idealised pressure signals at two traverse speeds: a nominal slow speed,  $v_1$ , at which the underlying signal is measured, and an arbitrarily fast speed,  $v_2$

Reconciling the two independent signals at differing traverse speeds on a sample-by-sample basis requires resampling to a common spatial axis. The transformation is then described by the spatial impulse response function

$$p_2(x) = h(x) * p_1(x)$$

$$h(x) * p_1(x) = \int_{-\infty}^{\infty} h(\varphi) p_1(x - \varphi) d\varphi \quad \#(17)$$

where  $p_1$  and  $p_2$  represent the traverse signals at speeds  $v_1$  and  $v_2$  respectively, and  $x$  represents distance in the direction of traverse motion. The discrete convolution sum of equation 5 is formed with each sample denoting a fixed position in space rather than an instant in time. Figure 11 shows an example of idealised pressure signals at two arbitrary traverse speeds.

The derivation of the inverse impulse response filter proceeds as before, using the new input-output pair:

$$\begin{aligned} p_2[n] &= h[n] * p_1[n] \\ \Rightarrow h[n] &= p_2[n] /* p_1[n] \#(18) \end{aligned}$$

$$(h[n])^{-1} * \delta[n] = (p_1[n] /* p_2[n]) * \delta[n] \#(19)$$

$$(h[n])^{-1} = \sum_{i=1}^N \frac{p_1[i]}{p_2[i]} \delta[n - i] \#(20)$$

The resulting spatial impulse response function, an example of which is given in Figure 12, is effectively a simple mapping of the temporal response function onto the spatial axis at the fixed speed  $v_2$ . Its application on a spatially-sampled basis relies on the data to be processed maintaining the fixed traverse speed  $v_2$  throughout, unlike time-based methods which account for varying traverse speed. This data is then resampled onto the same independent spatial axis, at the same spatial sample frequency, prior to application of the correction.

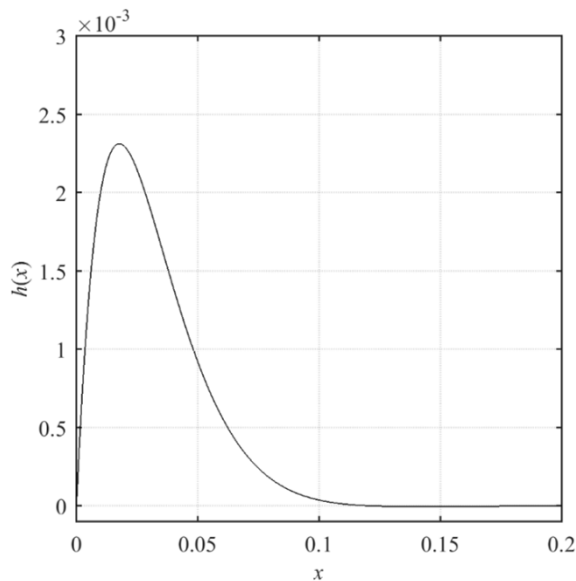


Figure 12: Example spatial-basis impulse response function derived from the idealised signals in Figure 11

### APPLICATION TO EXPERIMENTAL DATA

The impulse response functions are now applied to experimental traverse data, to demonstrate the effectiveness of the techniques. The traverse data were taken in the Engine Component Aerothermal (ECAT) facility at the University of Oxford (see Kirolos et al [18]), downstream of a cascade of turbine nozzle guide vanes (NGVs) operating at engine representative Reynolds and Mach numbers. The pressure measurement system is described by the “typical” system introduced earlier in this paper.

Figure 13 shows a comparison of uncorrected spatially resolved pressure signals obtained at a range of traverse speeds, from a low speed,  $v$ , at which all significant features should be fully resolved, to a high speed,  $6v$ , at which the signal is degraded due to the limited frequency response of the probe. The data cover two vane passages, and are normalised in traverse direction ( $x$ -axis) by the vane pitch. The pressure magnitude variation is normalised by the maximum pressure difference measured (maximum vane wake total pressure deficit) for the traverse at speed  $v$ , represented by one increment in the  $y$ -axis in the plot. For each speed, the data are averaged over four repeat passes in each direction to reduce the impact of random signal noise. The slowest traverse speed ( $v$ ) is further averaged between forward and reverse directions and gives a best estimate of the underlying signal. As the traverse speed increases, there is an increasing difference between the signals measured in the forward and reverse directions, and a degradation in the magnitude of the (negative) peak.

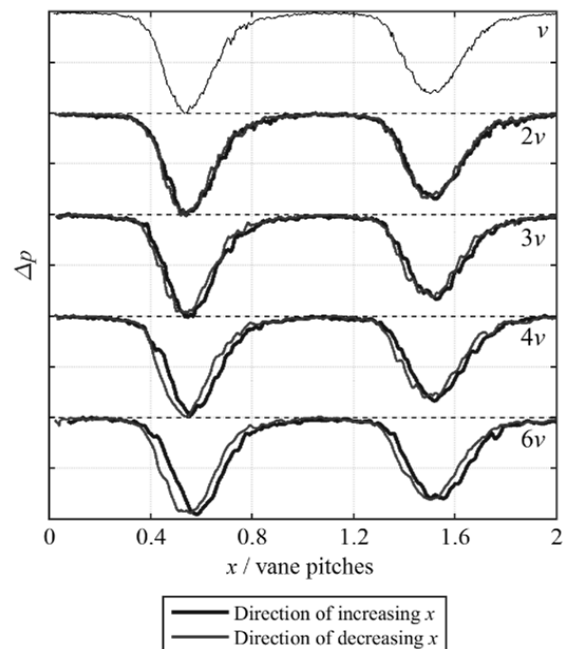


Figure 13: Uncorrected measured pressure traverse signals at five traverse speeds (averaged of four repeats per case)

To recover the underlying signals, the data at  $2v$ ,  $3v$ ,  $4v$  and  $6v$  were processed using the impulse response method using inverse impulse response filter functions derived using Methods 1 and 2.

Figure 14 shows recovered signals using Method 1 (theoretical system model), Model 3. Comparing the recovered signals with the underlying signal (traverse signal for speed  $v$ ), we can see that there is a good match for all traverse speeds, for recovered data in both the forward and reverse directions. That is, all recovered data collapse onto a single trend. This demonstrates both the accuracy and utility of the impulse response technique.

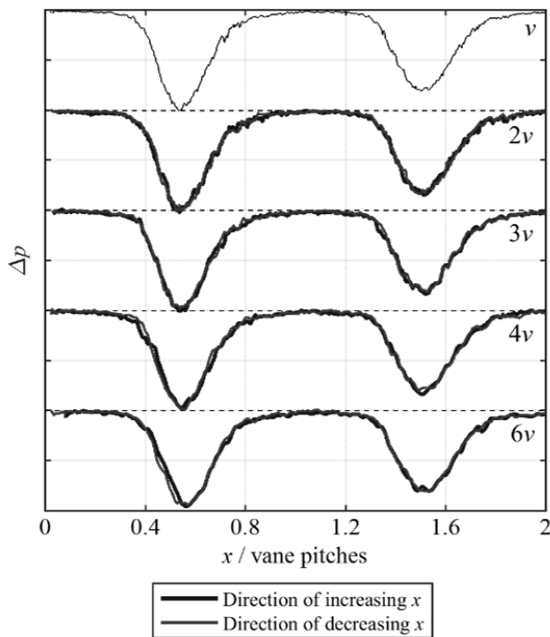


Figure 14: Impulse-response-corrected (Method 1, Model 3) measured pressure traverse signals at five traverse speeds

To quantitatively assess the quality of the recovered signals according to each of the three models used in Method 1 (theoretical system models), cross-correlations with the underlying signal are considered. Figure 15 shows examples of cross-correlation value plotted as a function of  $x$ -shift for each of the three models from Method 1, along with the uncorrected data, at traverse speed  $4v$ . The results for Models 1 and 3, both second order approximations of the example probe system, are indistinguishable at all traverse speeds tested, as shown in Figure 15.

The spatial shift between uncorrected traverses in opposing directions is greatly reduced in all corrected signals. This is evidenced by the corrected curves falling centrally between the uncorrected curves in Figure 15. This moves the value of spatial shift at which peak correlation occurs toward zero for all combinations of model

and traverse speed. The peak correlation value is also increased. Figure 16 shows trends in peak correlation with traverse speed for all methods of filter construction. The value achieved up to  $4v$  is very consistent before falling significantly at speed  $6v$ , suggesting that the accuracy of recovered signals may deteriorate at higher speeds. Further data at higher traverse speeds is required to confirm this.

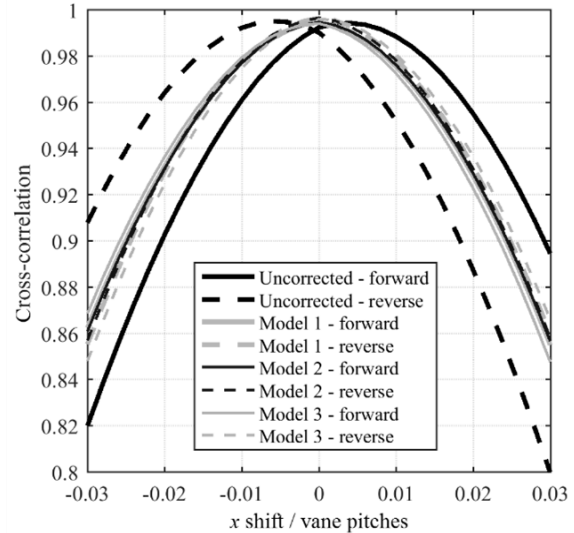


Figure 15: Cross-correlation between recovered signals at speed  $4v$  and the underlying signal (speed  $v$ ) using correction functions derived from each model of Method 1

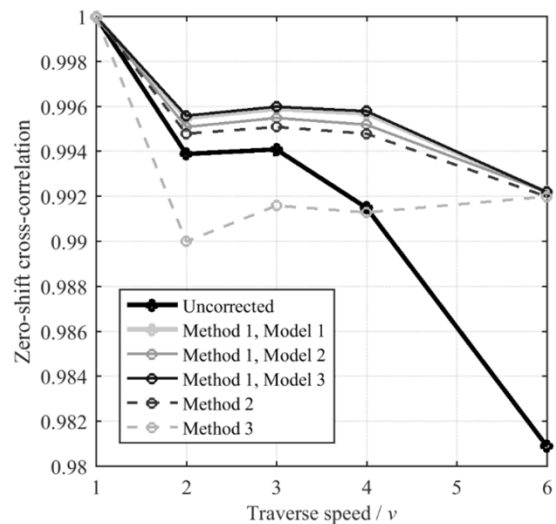


Figure 16: Values of cross-correlation with the underlying signal at zero shift achieved for the pressure system

Theoretical Model 3 marginally outperforms Model 2 at traverse speeds up to and including  $4v$ , while at  $6v$ , Model 2 offers the best result. It should be noted that only a single example pressure measurement system has been tested. It is known that the response—in particular the level of damping—is highly sensitive to the precise

geometry of the system. The relative simplicity of Model 3 is advantageous and its performance relative to the more complex Model 2 has been demonstrated to be very strong for moderately underdamped systems. For other systems, the accuracy of the predicted response should be evaluated by experimental means. Model 3 was therefore selected as the most suitable for this application, and is now compared against Methods 2 and 3.

The process for applying the spatial domain Method 3 is now described. The averaged traverse signals from Figure 13 are resampled onto a common spatial axis,  $x$ . The data at speeds  $2v$ ,  $3v$ ,  $4v$  and  $6v$  are in turn input as  $p_2(x)$  into Equation 20 and a transfer function is derived at each traverse speed to recover  $p_1(x)$ —the signal recorded at speed  $v$ . A second, independent set of traverse data is then obtained at each speed, averaged over three passes in each case.

The derived transfer functions are applied to the second data set using Equation 5 and the results are shown in Figure 17. The spatial shift of the data at high traverse speeds is again greatly reduced.

Figure 19 plots curves of cross-correlation between the underlying and recovered signals using each method of filter construction at traverse speed  $4v$ . The correlation curves from Methods 1 and 3 for opposing traverse directions overlaid almost perfectly. The impulse response filter of Method 3 was found to amplify high frequency noise on the signals being corrected. The values of correlation with the underlying signal are therefore much lower, although they do remain broadly constant with increasing traverse speed as shown in Figure 16, until at  $6v$  the correlation value matches the time-based models. At  $6v$ , the method benefits from the spatial filter being specifically determined at that speed. Where possible, the number of repeat passes included in the averaged signal used for

deriving the impulse response functions of Method 3 should be maximised, to minimise the impact of high frequency noise. Method 2 suffers to a lesser degree with the issue of noise amplification reducing peak correlation with the underlying signal. Additionally, the response filter from Method 2 fails to achieve the same agreement between recovered signals in opposite traverse directions.

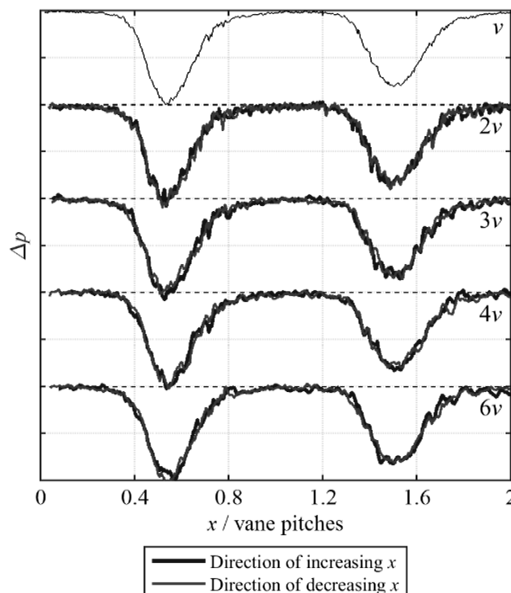


Figure 17: Pressure traverse signals at a range of traverse speeds, corrected with spatial inverse impulse response filters derived using Method 3

Finally, Figure 18 shows an example of a 2D contour plot of frequency-limited pressure traverse data, along with the corresponding plot transformed using the impulse response filter derived from theoretical Model 3. The uncorrected data shows clear spatial shifts in alternating directions

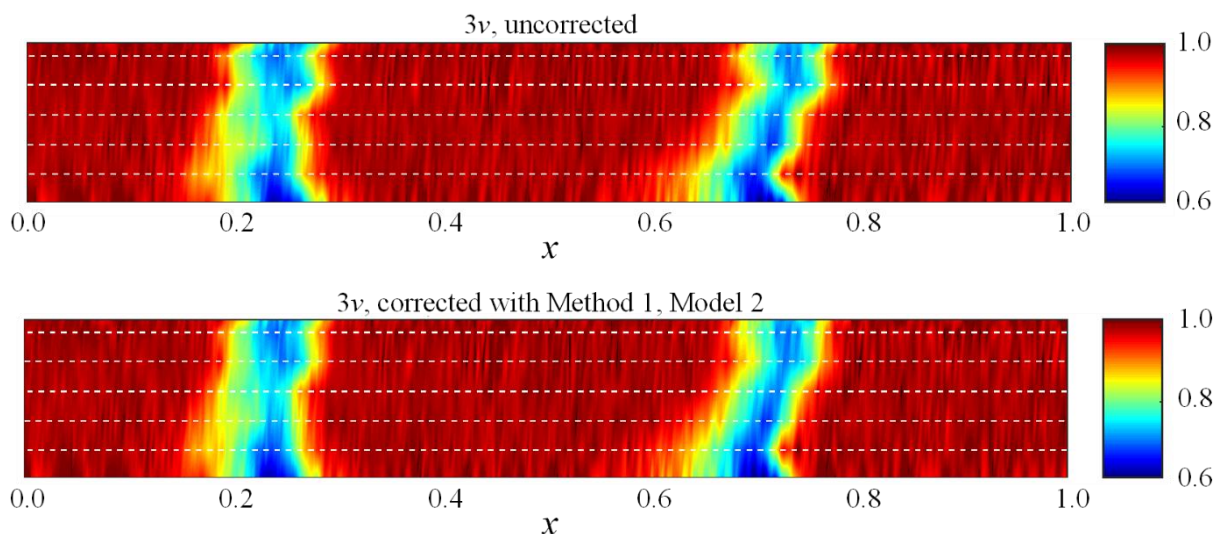


Figure 18: Example of a 2D contour plot of pressure data pre- and post-correction using the impulse response method

corresponding to the direction of traverse motion. The shift in the corrected data is much less visible and the wake boundaries are notably smoother. The remaining spatial shift is dominated by genuine variation in wake position.

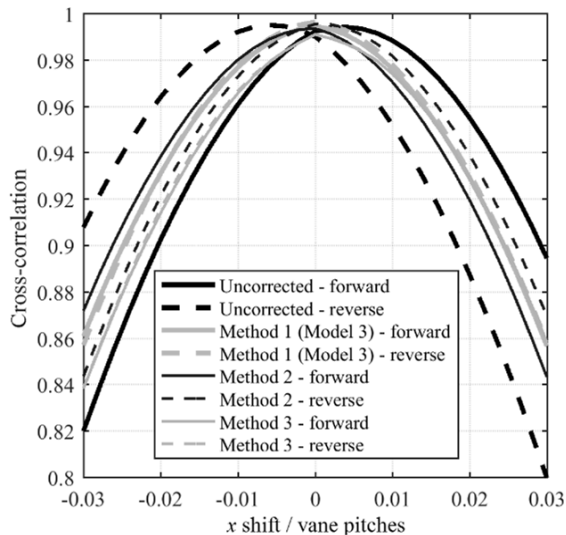


Figure 19: Cross-correlation between recovered signals at speed  $4v$  and the underlying signal (speed  $v$ ) using correction functions derived from each method

## CONCLUSIONS

In this paper it has been demonstrated that impulse response processing techniques can be used to improve the effective frequency response of pressure probes of the type used for traverse measurements in turbomachinery experiments. In practice the effective bandwidth (frequency cut-off limit) can be increased by a factor of approximately six, and further increases are likely to be possible with additional testing.

Three techniques for constructing the impulse response filter (required to apply the impulse response method) have been discussed: purely theoretical models; direct experimental characterisation; and a novel *multi-experiment in-situ characterisation method* requiring neither direct experimental *system* characterisation nor complete system information. The novel method uses a series of experiments of the unknown flow (system being measured) performed at different traverse speeds. The system impulse response filter is defined as that which best recovers the underlying signal from the observed (input) signals.

All three techniques have been shown to be sufficiently accurate in practical situations to construct accurate impulse response filters. The choice of the optimum technique for a given application will depend largely on practical issues, for example the relative ease with which a direct experimental system characterisation can be performed, or the degree to which the required system information to construct a theoretical model

is available, or finally, the ease with which a series of test data for the *multi-experiment in-situ characterisation method* could be collected.

Impulse response techniques are well established in signal processing, but seldom used in aerodynamics research. The practical value of this technique—which allows higher frequencies than the ‘natural’ limit of the probe to be resolved, thus expanding the frequency and wavenumber ranges over which probes can be used—should be self-evident to researchers in the fields of aerodynamics and turbomachinery.

## REFERENCES

- [1] Holmes, J. D.; Lewis, R. E.; 1986. “Optimisation of Dynamic Pressure Measurement Systems”. I. Single Point Measurements, *J. Wind Eng. Industrial Aero.*, 25(1987) 249-273
- [2] van Ommen, J. R.; Schouten, J. C.; van der Stappen, M. L. M.; van den Bleek, C. M.; 1999. “Response Characteristics of Probe-Transducer Systems for Pressure Measurements in Gas-Solid Fluidised Beds: How to Prevent Pitfalls in Dynamic Pressure Measurements”. *Powder Technology*, 106(1999) 199-218
- [3] Hooper, J.D.; Musgrove, A. R.; 1997. “Reynolds Stress, Mean Velocity, and Dynamic Static Pressure Measurement by a Four-Hole Pressure Probe”. *Experimental Thermal and Fluid Science* 1997, 15:375-383
- [4] Paniagua, G.; Dénos, R.; 2002. “Digital Compensation of Pressure Sensors in the Time Domain”. *Experiments in Fluids*, 32(2002) 417-424
- [5] Forney, L. J.; Fralick, G. C.; 1994. “Two wire thermocouple: Frequency response in constant flow”. *Rev. Sci. Instrum.* 65, 3252 (1994)
- [6] Tagawa, M.; Ohta, Y.; 1997. “Two-thermocouple probe for fluctuating temperature measurement in combustion—Rational estimation of mean and fluctuating time constants”. *Combustion and Flame*, Vol. 109, pp 549-560
- [7] Braun, J.; Lu, S.; Paniagua, G.; 2017. “Development of high frequency virtual thermocouples”. *Proceedings of ASME Turbo* 2017, Paper No. GT2017-64669
- [8] Oldfield, M. L. G.; 2008. “Impulse response processing of transient heat transfer gauge signals”. *ASME Journal of Turbomachinery*, April 2008, Vol. 130 / 021023-1
- [9] Lubbock, R. J.; Luque, S.; Rosic, B. R.; 2018. “A New Transient High Heat Flux Convection Calibration Facility for Heat Transfer Gauges in High Enthalpy Flows”. *ASME J. Heat Transfer*, 140(4), 041701

- [10] Lubbock, R. J.; 2014. "Turbulent Velocity and Temperature Measurements in Gas Turbine Hot Sections". DPhil thesis, University of Oxford, UK
- [11] Stepanishen, P. R.; Fisher, G.; 1981. "Experimental Verification of the Impulse Response Method to Evaluate Transient Acoustic Fields". *J. Acoust. Soc. Am.*, 69(6), June 1981
- [12] Oldfield, M. L. G.; 2000. "Guide to Impulse Response Heat Transfer Signal Processing". OUEL Report 2233/2000, University of Oxford, UK
- [13] Bajsić, I.; Kutin, J.; Žagar, T.; 2007. "The response time of a pressure measurement system with a connecting tube". *Instrumentation Science and Technology*, 35(4), pp 399-409 (doi: 10.1080/10739140701436579)
- [14] Hall, B. F.; Povey, T.; 2018. "A practical model for pressure probe system response estimation (with review of existing models)". *Meas. Sci. Technol.*, 29(4),
- [15] Bergh, H.; Tijdeman, H.; 1965. "Theoretical and experimental results for the dynamic response of pressure measuring systems". NLR Technical Report F.238, National Aero- and Astronautical Research Institute
- [16] Richards, W. B.; 1986. "Propagation of sound waves in tubes of non-circular cross section". NASA Technical Paper 2601
- [17] Yang, W. C.; Tobler, W. E.; 1991. "Dissipative modal approximation of fluid transmission lines using linear friction model". *J. Dyn. Syst. Meas. Control*, 113(1), pp 152-162
- [18] Kirollos, B.; Lubbock, R.; Beard, P.; Goenaga, F.; Rawlinson, A.; Janke, E.; Povey, T.; 2017. ECAT: An engine component aerothermal facility at the University of Oxford, Proceedings of ASME Turbo Expo 2017, Paper No. GT2017-647